doi:10.1016/j.jmb.2011.07.054 J. Mol. Biol. (2011) 413, 150–161

Contents lists available at www.sciencedirect.com

Journal of Molecular Biology

journal homepage: http://ees.elsevier.com.jmb

Improving the Resistance of a Eukaryotic β-Barrel Protein to Thermal and Chemical Perturbations

Dennis Gessmann[1], Frauke Mager[1,2], Hammad Naveed[3], Thomas Arnold[2], Sara Weirich[1], Dirk Linke[2], Jie Liang[3] and Stephan Nussberger[1]*

[1]*Biophysics Department, Institute of Biology, University of Stuttgart, Pfaffenwaldring 57, 70550 Stuttgart, Germany*
[2]*Department of Protein Evolution, Max Planck Institute for Developmental Biology, Spemannstraße 35-39, 72076 Tübingen, Germany*
[3]*Department of Bioengineering, University of Illinois, 835 South Wolcott, Chicago, IL 60612, USA*

Received 4 March 2011;
received in revised form
22 July 2011;
accepted 23 July 2011
Available online
29 July 2011

Edited by J. Bowie

Keywords:
β-barrel;
Tom40;
apparent protein stability;
protein engineering;
TOM complex

β-Barrel membrane proteins have regular structures with extensive hydrogen-bond networks between their transmembrane (TM) β-strands, which stabilize their protein fold. Nevertheless, weakly stable TM regions, which are important for the protein function and interaction with other proteins, exist. Here, we report on the apparent stability of human Tom40A, a member of the "mitochondrial porin family" and main constituent of the mitochondrial protein-conducting channel TOM (*t*ranslocase of the *o*uter *m*embrane). Using a physical interaction model, TmSIP, for β-barrel membrane proteins, we have identified three unfavorable β-strands in the TM domain of the protein. Substitution of key residues inside these strands with hydrophobic amino acids results in a decreased sensitivity of the protein to chemical and/or thermal denaturation. The apparent melting temperature observed when denatured at a rate of 1 °C per minute is shifted from 73 to 84 °C. Moreover, the sensitivity of the protein to denaturant agents is significantly lowered. Further, we find a reduced tendency for the mutated protein to form dimers. We propose that the identified weakly stable β-strands 1, 2 and 9 of human Tom40A play an important role in quaternary protein–protein interactions within the mammalian TOM machinery. Our results show that the use of empirical energy functions to model the apparent stability of β-barrel membrane proteins may be a useful tool in the field of nanopore bioengineering.

Introduction

The transmembrane (TM) domains of β-barrel membrane proteins have regular structures with an extensive hydrogen-bond network between the individual β-strands.[1,2] Despite this strong network, unfavorable or weakly stable regions exist in several β-barrel membrane proteins.[3,4] They are often important for their function, such as voltage sensing,[5] flux control of metabolites and ion sensing (see Refs. 6 and 7 for detailed reviews).

In general, β-barrel membrane proteins are stabilized through binding of α-helices to weakly stable regions inside or outside of the pore, so-called in-plugs or out-clamps, through formation of oligomers via protein–protein interfaces or interactions with lipids.[3,4,6,8]

*Corresponding author. E-mail address: nussberger@bio.uni-stuttgart.de.

Abbreviations used: TM, transmembrane; hTom40A, human Tom40A; AfTom40, Tom40 from *Aspergillus fumigatus*; LDAO, lauryldimethylamine-oxide; GnHCl, guanidine hydrochloride; wt, wild type; IB, inclusion bodies.

In this work, we explore whether the prediction of weakly stable regions in bacterial β-barrels[3,4] can be adapted to human Tom40A (hTom40A) and reveal further insights on the structural organization of this protein.

In eukaryotes, Tom40 proteins represent an essential class of pore proteins that facilitate the translocation of unfolded proteins from the cytosol into mitochondria. They comprise the main subunit of the TOM (*t*ranslocase of the *o*uter *m*embrane) import machinery in mitochondrial outer membranes.[9–14]

It is generally predicted that all eukaryotic Tom40 proteins belong to the "mitochondrial porin" superfamily. Thus, hTom40A most likely constitutes a β-barrel architecture similar to that of VDAC-1 with 19 β-strands and a short α-helix located inside the pore.[15–17] Consistent with this model, circular dichroism (CD) and Fourier transform infrared secondary structure analyses of Tom40 and VDAC proteins from different organisms revealed a dominant β-sheet structure with a small α-helical part.[9,18,19]

In the present study, we calculated the energy of each amino acid in the predicted native conformation of hTom40A using a recently introduced empirical potential function that was developed based on extensive combinatorial analysis of known bacterial β-barrel membrane protein structures.[3] We have identified three β-strands (1, 2 and 9) in the TM domain of hTom40A that contribute to the overall sensitivity of the protein to denaturation. We show that mutagenesis of the predicted specific destabilizing amino acid residues within these strands leads to a higher resistance to thermal or chemical perturbation of the barrel. Similar results were obtained with Tom40 from *Aspergillus fumigatus* (AfTom40). We propose that the unstable β-strands 1, 2 and 9 of the TM domain of hTom40A interact with other Tom40 molecules or subunits of the TOM complex.

Results

Weakly stable regions in hTom40A and oligomerization index

The stability of β-barrel membrane proteins is determined by the balance between favorable hydrogen-bond networks, van der Waals and hydrophobic interactions and unfavorable conformational entropy. To identify weakly stable regions in the TM domain of wild-type (wt) hTom40A (Fig. 1a and b), we estimated the energetic contribution of all amino acid residues to the β-strand stability of the protein by using a computational approach[3] that has recently been applied to model the conformational stability of 25 nonhomologous β-barrel membrane proteins of known structure. Briefly, we calculated the energetics of embedding specific residue types at different regions of the TM domain, the stabilizing effect due to interactions between residues on neighboring strands through strong H-bond, weak H-bond and side chain–side chain interactions using the updated TmSIP empirical energy parameters.[3,20]

We calculated the contribution of residues to the empirical energy for each β-strand (Fig. 1c). Strands 1, 2 and 9 have significantly higher empirical energies and are thus less favorable than the rest of the protein. Then, the oligomerization index ϱ_{wt}, which summarizes the energy deviation of unstable strands from the expected energy value for all the strands in the protein, was calculated to be $\varrho_{wt} = 2.48$. This is in good agreement with the observation that highly unfavorable strands are often associated with protein–protein interfaces in the TM region.

In data sets using sequence information of bacterial β-barrel membrane proteins, a protein can be predicted to be monomeric if the oligomerization index is <2.25 and oligomeric if it is >2.75.[3] The oligomerization index of hTom40A is between these prediction thresholds. Theoretically, wt hTom40A may thus exist as stable monomers but may also form higher-order complexes through distinct protein–protein interaction interfaces.

We further examined the contribution of all amino acids facing the membrane lipids within the predicted three unfavorable strands 1, 2 and 9 (Fig. 1d). In this analysis, residues K107 in strand 1, H117 in strand 2 and H220 in strand 9 were found to contribute the most to the instability of these strands. Based on our calculations, we predict strands 1, 2 and 9 of hTom40A to be unfavorable/weakly stable. Each strand can have two orientations: the side chain of the first residue can face either the lipid environment or the internal of the barrel. The orientations of strands are predicted using the energy scale in Ref. 3 such that the number of costly burial of ionizable/polar residues facing the lipid environment is overall minimized.

Secondary and tertiary structures of hTom40A

In order to account for the differences between bacterial and mitochondrial β-barrel membrane proteins and keeping in mind that hTom40A forms complexes also with other components of the TOM machinery, we wanted to construct a mutant protein to have an oligomerization index ϱ below 1.5 so that the resulting mutant hTom40A would form more stable monomers, possibly without protein–protein interaction interfaces.

To test to what extent do β-strands 1, 2 and 9 determine the overall resistance to denaturation and oligomerization state of hTom40A, we designed five mutants, termed K107L, H117L, H220L, K107L/H117L and K107L/H117L/H220L, where residues K107, H117 and H220 of hTom40A are replaced by

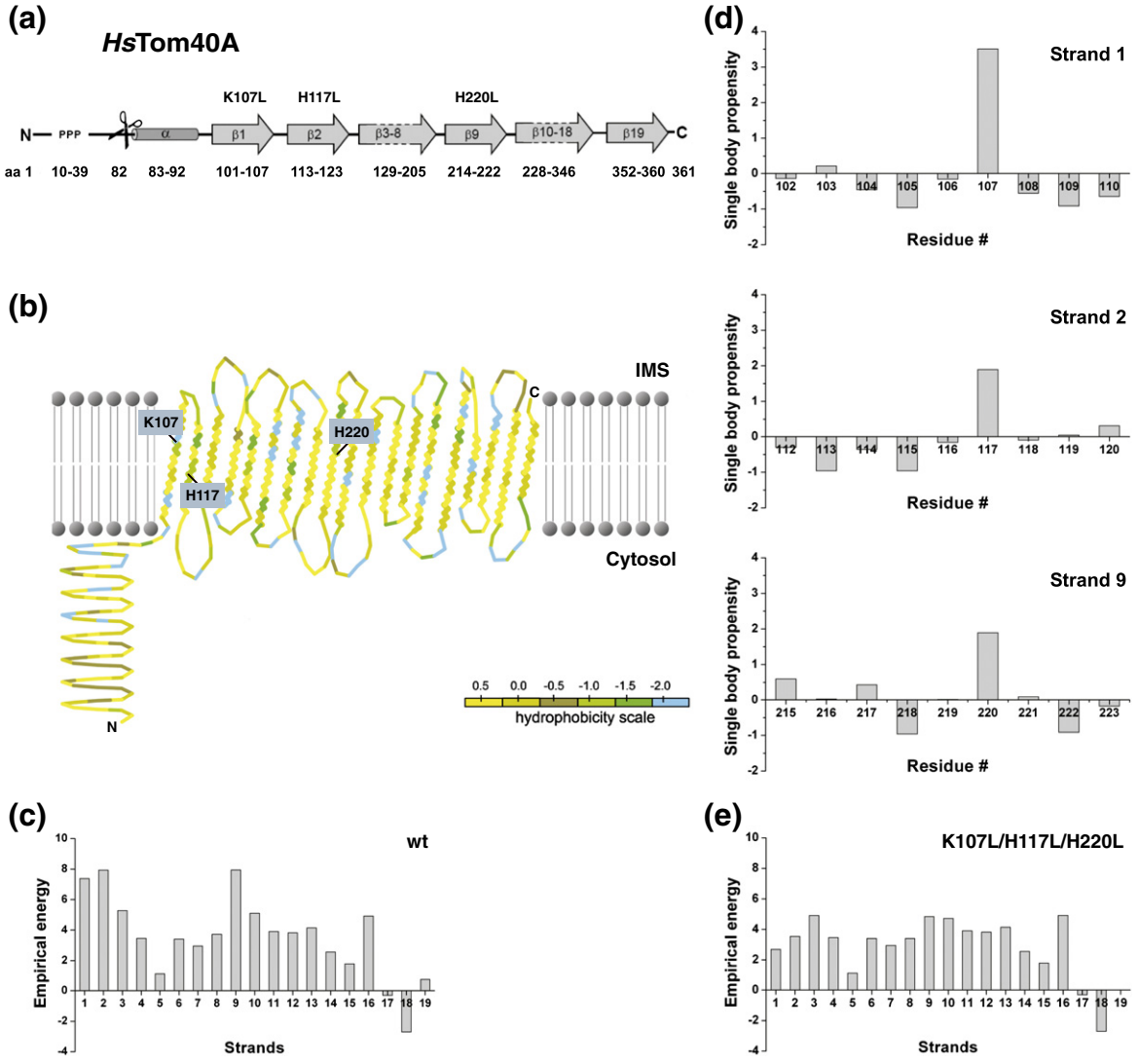

Fig. 1. Expected energy levels of strands and residues in the TM domain of hTom40A. (a) The secondary structure prediction of hTom40A is based on PRED-TMBB[30] and TMBETAPRED-RBF.[31] (b) The protein topology of hTom40A was generated using TMRPres2D.[48] (c) Empirical energy of β-strands 1–19 of wt protein. β-Strands 1, 2 and 9 are predicted as the weakly stable strands. (d) Single-body propensities of amino acid residues of the TM domains of β-strands 1, 2 and 9. Amino acids K107, H117 and H220 show the highest values, indicating a destabilizing effect on the regarding strand. (e) Empirical energy of β-strands 1–19 of mutant (K107L, H117L and H220L) hTom40A.

leucines. Leucine is predicted to be the most stabilizing amino acid when facing the lipid within the core region of a TM β-strand.[3]

The empirical energy profile of the triple mutant hTom40A^{mut} (K107L/H117L/H220L) is shown in Fig. 1e. The oligomerization index of this mutant ($\varrho_{K107L/H117L/H220L}=1.37$) was significantly lower than that of the wt protein ($\varrho_{wt}=2.48$), predicting a very robust monomeric β-barrel membrane protein. Energy calculations of single and double mutants revealed higher indices ($\varrho_{K107L}=2.08$, $\varrho_{H117L}=2.01$, $\varrho_{H220L}=2.03$, $\varrho_{K107L/H117L}=1.91$, $\varrho_{K107L/H220L}=1.71$ and $\varrho_{H117L/H220L}=1.68$), predicting less stable proteins.

Mammalian Tom40A isoforms show a very high sequence identity among each other (>91%, data not shown). All include a remarkable N-terminal poly-proline region, which is only present in mammalian Tom40A. So far, thermal stability analyses of the TM β-barrels of mammalian full-length Tom40A proteins using UV CD spectroscopy have not been successful in our hands (data not shown). The β-barrel UV CD signals appeared to be superimposed by strong CD signals caused by the poly-proline-rich region of the protein. As a consequence of this interference, temperature-induced transitions of the β-barrel itself could not be monitored accurately. Since the N-terminal poly-proline-rich domain in

mammalian Tom40A proteins has no effect on the channel formation,[21] we deleted the poly-proline region of all hTom40A proteins to improve the CD signal in heat-induced unfolding measurements.

wt and mutant Tom40A proteins were expressed in *Escherichia coli* and nickel affinity purified from inclusion bodies (IB) under denaturing conditions. The proteins were refolded by rapid dilution of denaturant into lauryldimethylamine-oxide (LDAO)-containing detergent buffer and further purified via size-exclusion chromatography. Analysis of refolded proteins by SDS-PAGE and Coomassie and silver staining (Fig. 2a) indicated that all isoforms were virtually pure. Far-UV CD spectroscopy showed typical β-barrel spectra for wt and mutant proteins with similar curves for all hTom40A isoforms[9,10,18,21] (Fig. 2b). The spectral characteristics of the wt hTom40A and the triple mutant are summarized in Supplementary Table 2. At wavelengths >250 nm, the CD spectra approached ellipticity values close to 0, indicating that the protein preparations were virtually free of higher- order aggregates, which would cause light- scattering effects and interfere with the interpretation of the data.

Further, tertiary structure was analyzed via tryptophan fluorescence spectroscopy. The emission spectra of wt and all mutant Tom40 proteins (Fig. 2c) were exactly the same, with intensity maxima at approximately 340 nm and an unchanged width of the emission spectra. This can be interpreted as an unaltered environment of the widely spread tryptophan residues, W188, W259 and W322, which are conserved in the amino acid sequence of all isoforms and remain unchanged in all our designed mutant proteins. In summary, we suggest that secondary and tertiary structures match in all hTom40A isoforms and, consequently, differences in resistance to chemical and thermal perturbations and oligomerization state are not due to an altered protein structure.

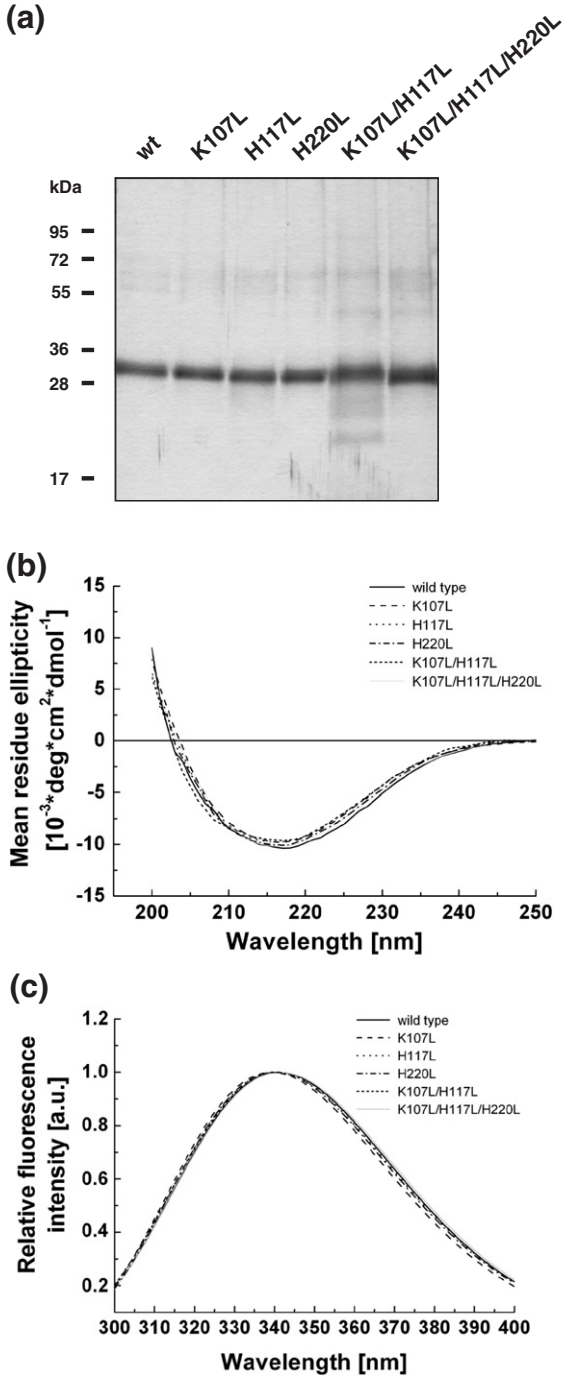

Fig. 2. Far-UV CD spectra and tryptophan fluorescence emission spectra of wt and mutant hTom40A. (a) SDS-PAGE showing purified wt and mutant (K107L, H117L, H220L, K107L/H117L and K107L/H117L/H220L) hTom40A. Proteins were visualized by silver staining. (b) Comparison of far-UV CD spectra between wt and mutant hTom40A. Measurements were carried out at a protein concentration of ~0.2 mg/ml in 1% (w/v) LDAO at 25 °C for wt and mutant proteins, respectively. For each experiment, five scans were accumulated at the indicated temperatures. Noisy data below 200 nm due to optical density have been removed. (c) Comparison of tryptophan fluorescence emission spectra of wt and mutant hTom40A. Emission spectra were conducted in 20 mM Tris–HCl (pH 8), 1% (w/v) LDAO, 1 mM β-mercaptoethanol and 350 mM GnHCl at a protein concentration of ~0.15 mg/ml for all isoforms. Data points were fitted to the log-normal distribution as described in Materials and Methods. Relative fluorescence intensity is in arbitrary units (a.u.). All isoforms exhibit the exact same far-UV CD and tryptophan fluorescence emission spectra characteristics. We suggest analogue β-barrel formation for wt and mutant hTom40A.

Thermal and solvent stability of hTom40A

To compare the thermal stability of wt and mutant hTom40A, we measured CD signals at different

temperatures at constant wavelength. wt hTom40A unfolded at an apparent melting temperature of about 73 °C when denatured at a rate of 1 °C per minute (Fig. 3). In line with our energy calculations described above, hTom40A with substitutions at positions K107, H117 and H220 revealed an apparent midpoint of resistance to thermal denaturation of approximately 84 °C (Fig. 3). The single and double mutants appeared to be slighty more stable than wt protein; however, differences proved not to be significant (data not shown).

To provide further evidence that substitution of unfavorable amino acids in the TM domain of hTom40A results in conformational stabilization of the protein, we compared tryptophan fluorescence spectra of wt and mutated hTom40A in the presence of chemical denaturants. The change in tryptophan fluorescence of wt and mutated hTom40A, respectively, was monitored at different guanidine hydrochloride (GnHCl) concentrations (Fig. 4a and b). wt Tom40 was completely denatured in ~5 M GnHCl. The apparent midpoint of unfolding occurred at a concentration of ~3.1 M GnHCl. On the other hand, the resistance of mutant Tom40 K107L/H117L/H220L to chemical denaturation was greatly enhanced (Fig. 4c). The apparent midpoint of unfolding of hTom40A was shifted from 3.1 to approximately 4.8 M GnHCl. Mutant hTom40A K107L/H117L/H220L completely unfolded at ~6.3 M GnHCl. These results were obtained

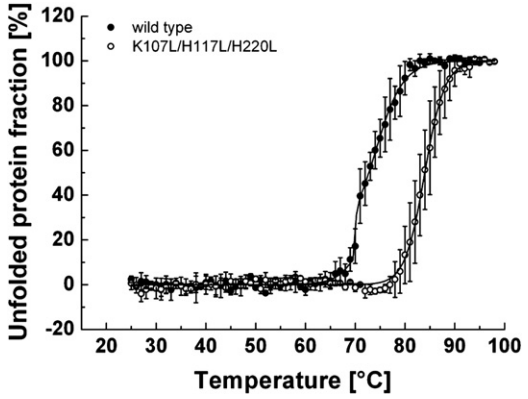

Fig. 3. Sensitivity of wt and mutant hTom40A to thermal denaturation. Thermal denaturation of both hTom40A isoforms was monitored under the same conditions as described in Fig. 2b by change in ellipticity at 216 nm. wt and mutant proteins were subjected to temperature increases of 1 °C/min from 25 to 98 °C, respectively. Data points of melting curves were normalized to the minimum and maximum percentages of unfolded protein fraction ($n=3$, error bars=SD)[49] and then fitted to sigmoid functions (black line). Apparent melting temperatures were retrieved at the midpoint of the transition curves. wt Tom40A indicated a three-state unfolding mechanism, whereas the triple mutant hTom40A showed a two-state unfolding mechanism with an approximately 11 °C higher apparent melting temperature.

whether unfolded or refolded Tom40 was incubated with GnHCl (Fig. 4c and d), showing the reversibility of the chemical denaturation.

Chemical unfolding of hTom40A K107L, H220L, H117L and K107L/H117L occurred at around 2.9, 3.5, 3.9 and 4.2 M GnHCl (Fig. 4c). These mutants were thus more resistant to chemical denaturation than wt hTom40A but less resistant than the triple mutant K107L/H117L/H220L. Our data indicate that the resistance of the mutants to chemical denaturation increased with decreasing ϱ-values. They further suggest that wt hTom40A unfolds via a multistate mechanism, whereas unfolding of "stabilized" protein follows a two-state conformational transition.

Thermal and solvent stability of AfTom40

To further test the prediction of weakly stable β-strands in eukaryotic porins, we applied stability calculations to full-length AfTom40. Comparison of full-length AfTom40 and wt hTom40AΔ1–82 revealed a moderate identity at the amino acid level (~25% identical residues in the conserved TM part, including the N-terminal helix) but a similar β-barrel secondary structure (Supplementary Fig. 1). We identified five unstable regions in AfTom40 to compromise the stability of β-strands 1, 5–7, 9, 13 and 17 (Fig. 5a). The ϱ-value of the wt protein was calculated to be 2.81. To see to what extent do these β-strands determine the stability of the protein, we made an AfTom40 variant with mutations K69H, N150H, S180L, S236A and K302H. These mutated residues were predicted to be the most favorable residues in the respective positions of the β-strand by the TmSIP potential function. The ϱ-index of this mutant was calculated as 1.66 (Fig. 5a). wt and mutant AfTom40 were over-expressed in *E. coli* cells, purified under denaturing conditions and refolded into polyoxyethylene monolauryl ether (Brij35)-detergent containing buffer in a similar way as hTom40A (Fig. 5b). Far-UV CD spectra of both proteins (Fig. 5c) showed a β-barrel fold as for hTom40A. Tryptophan fluorescence emission spectra were also almost identical, supporting a similar structure for both AfTom40 proteins (Fig. 5d). Thermal denaturation of both AfTom40 proteins followed by CD spectroscopy revealed no difference in the apparent melting temperature but a clear change in the cooperativity in unfolding (Fig. 5e). In contrast to thermally induced unfolding, chemically induced unfolding of wt and mutant AfTom40 proteins revealed an apparent stabilization of the mutant protein (Fig. 5f). The apparent midpoint of unfolding of wt protein was observed around 2.5 M and was shifted to about 3.2 M GnHCl in the mutant protein. Both patterns of unfolding were in line with those observed for thermal unfolding (Fig. 5e) and those observed for hTom40A (Fig. 4c and d).

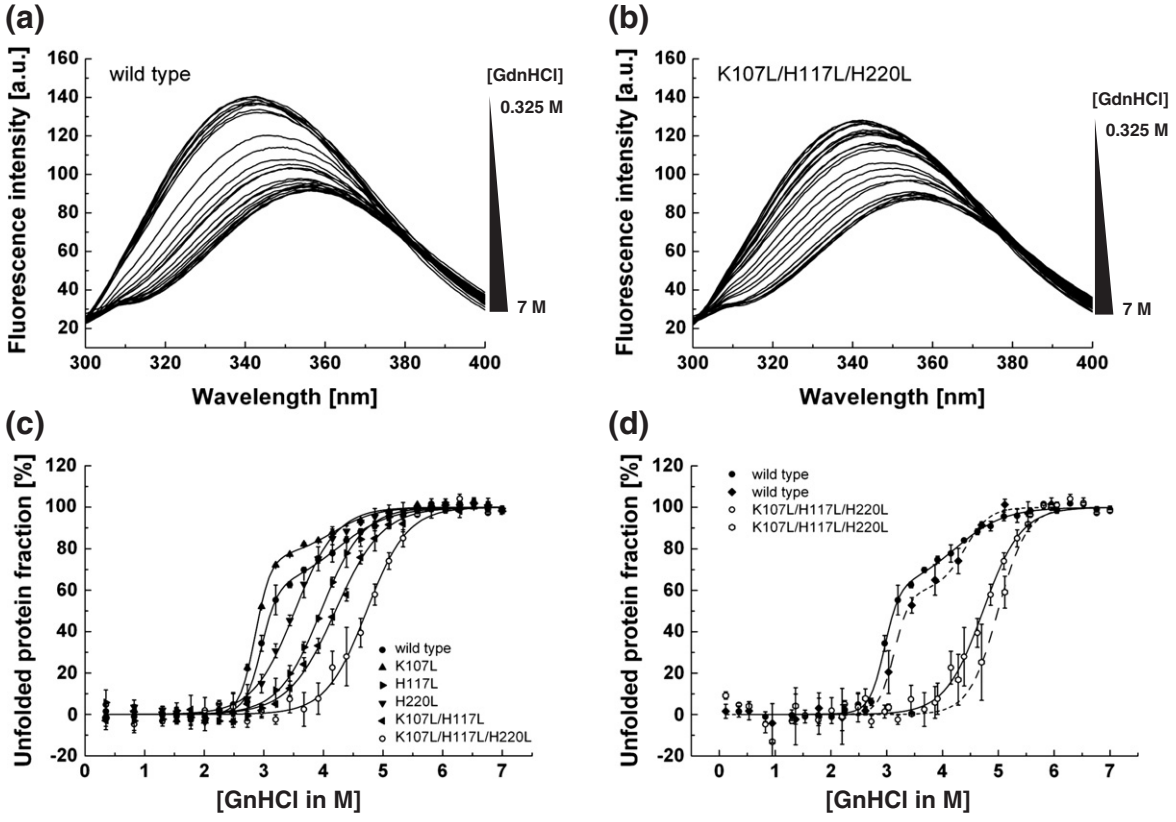

Fig. 4. Sensitivity of wt and mutant hTom40A to chemical denaturation. (a and b) Tryptophan fluorescence emission spectra of wt and mutant hTom40A (~0.15 mg/ml) were recorded in Tris–HCl buffer containing 1% LDAO after 24 h of incubation with GnHCl at 25 °C. GnHCl concentrations varied from 0.35 to 7 M, respectively. (c) The fractions of unfolded wt and mutant Tom40 were determined at different GnHCl concentrations from fluorescence intensities recorded at 330 nm relative to a denatured protein solution. (d) To show the reversibility of the chemical unfolding, we repeated the experiment by subjecting folded wt and mutant K107L/H117L/H220L hTom40A to increasing GnHCl concentrations (dashed lines). For comparison, we included the data from the refolding reaction in panel (c) (solid lines). The figures in (c) and (d) show an average of three independent experiments (error bars=SD).

Oligomerization states of hTom40A

Previous studies revealed that weakly unfavorable regions in bacterial β-barrel proteins can be stabilized through oligomerization of monomers.[3] Our energy calculations described above predicted a very stable monomeric form for the mutant hTom40A K107L/H117L/H220L. To verify this hypothesis, we conducted chemical cross-linking experiments on both wt and triple mutant Tom40 solubilized in LDAO. Both protein samples were incubated with glutaraldehyde, which forms covalent bonds between primary amine groups. The degree of intermolecular cross-link formation was evaluated by SDS-PAGE and Western blotting (Fig. 6). wt hTom40A was present mostly in its monomeric form but also formed dimers. In contrast, mutant protein was predominantly monomeric and revealed virtually no dimers. Similar results were obtained with proteins in β-dodecylmaltoside-containing buffer (data not shown).

It should be noted, however, that long exposures of both proteins to glutaraldehyde resulted in protein aggregates that did not enter the SDS gel. In summary, we conclude successful stabilization of the hTom40A β-barrel. Hence, for mutant hTom40A K107L/H117L/H220L, oligomerization is not required to compensate for unfavorable regions.

Discussion

In this study, we applied a recently developed method for the prediction of unfavorable regions in bacterial β-barrel membrane proteins[3] to eukaryotic hTom40A. We identified and experimentally confirmed two regions in the TM domain of the protein (β-strands 1 and 2 and β-strand 9) that have strong impact on its resistance to thermal and chemical perturbations. Oligomerization of hTom40A monomers might provide the mechanism to counterbalance the overall β-barrel instability, indicating

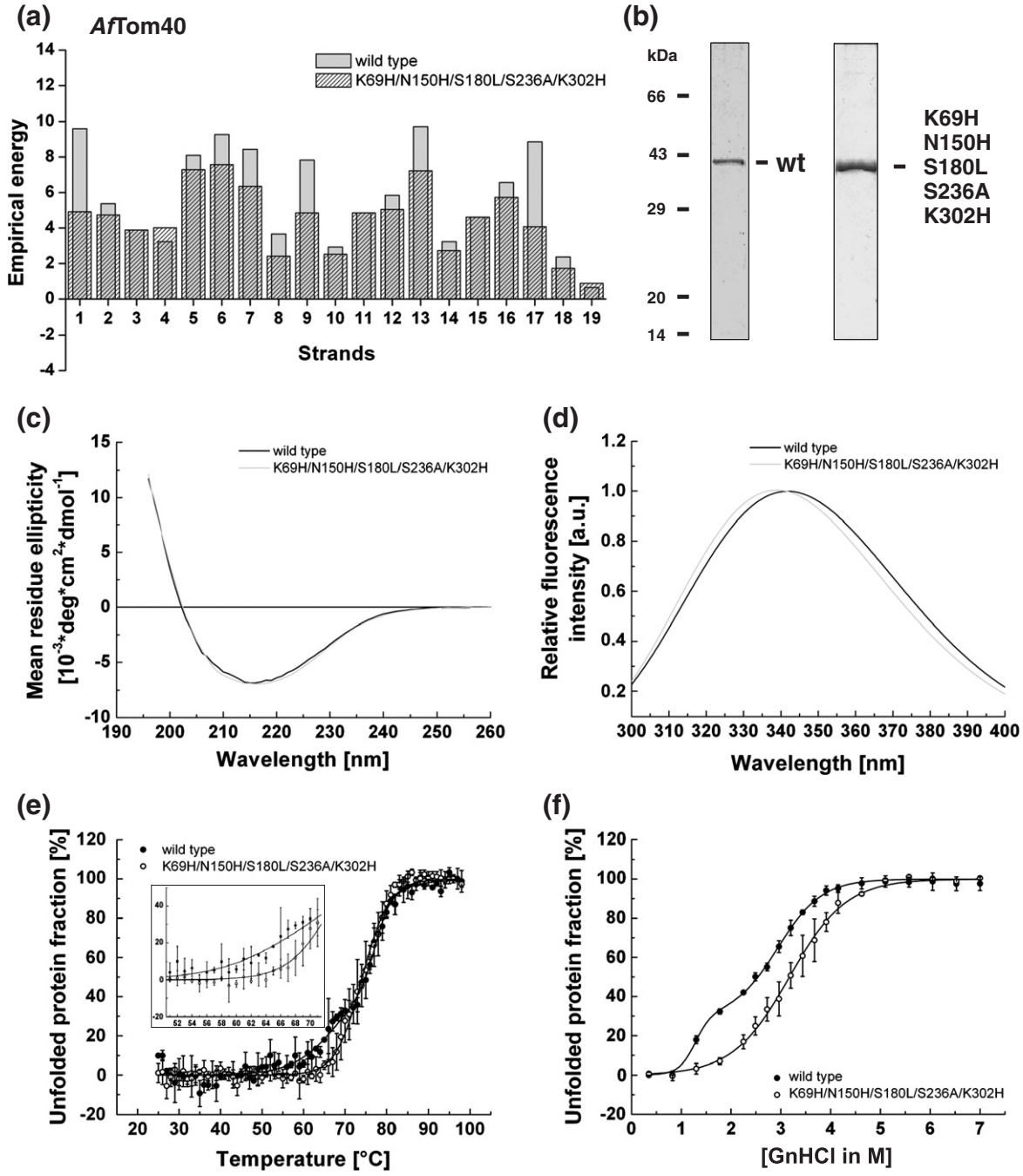

Fig. 5. Stability analysis of AfTom40. (a) Empirical energy of β-strands 1–19 of wt and mutant proteins. (b) SDS-PAGE of purified and refolded wt and mutant (K69H, N150H, S180L, S236A and K302H) AfTom40 throughout Coomassie Blue staining. Far-UV CD spectra (c) and tryptophan fluorescence emission spectra (d) of AfTom40 wt/mutant were recorded and deconvoluted as described in Fig. 2, respectively. Both AfTom40 isoforms adapt the same secondary structure (c), but mutant AfTom40 showed an approximately 1.5-nm left-shifted tryptophan fluorescence emission spectrum. Thermal (e) and chemical (f) sensitivities of AfTom40 isoforms were investigated according to Figs. 3 and 4c. Thermal and GnHCl-induced unfolding of proteins revealed a three-state unfolding mechanism for the wt and a two-state unfolding mechanism for the mutant protein with a higher stability for the mutated form of AfTom40.

possible protein–protein interfaces in mammalian Tom40 proteins. Indeed, the existence of dimeric and trimeric Tom40 forms was shown for fungal Tom40.[22,23] However, for mammalian Tom40 proteins, experimental evidence has yet to be shown. Nevertheless, our results suggest that β-strands 1, 2

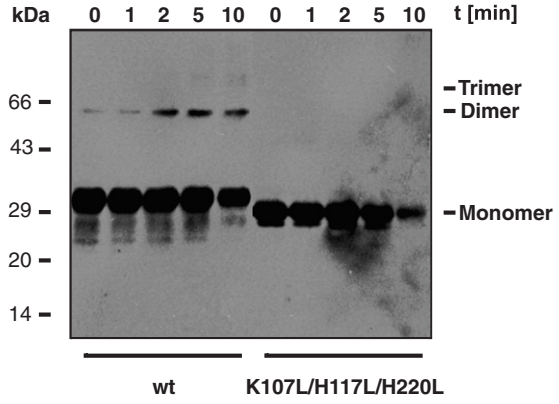

Fig. 6. Chemical cross-linking of refolded wt and mutant (K107L, H117L and H220L) hTom40A. wt and mutant proteins (40 μM) were incubated with glutaraldehyde (125 μM) at 37 °C in 20 mM NaH_2PO_4, pH 8. Aliquots were taken after the addition of the cross-linking reagent at the time indicated. In these, cross-linking reactions were stopped by addition of 50 mM Tris, pH 8. Proteins and cross-linking products were visualized by SDS-PAGE and Western blotting.

and 9 in the TM domain of mammalian Tom40 might be important for the association of single Tom40 molecules. In addition, other subunits of the mitochondrial protein import machinery TOM, for example, the small Tom proteins, might also interact with β-strands 1, 2 and 9 in the TOM complex from mammals.[24]

Interestingly, the key amino acids K107, H117 and H220 in the two unfavorable regions of hTom40A are not strongly conserved between different species (e.g., fungi and plants). This and the results of our stability calculations for AfTom40 indicate that weakly stable regions in mammalian Tom40 proteins differ from evolutionarily more distant Tom40 β-barrels.

Using the described method above for the prediction of unfavorable regions on fungal AfTom40, we identified five unstable domains comprising strands 1, 5–7, 9, 13 and 17. As in the case of mammalian TOM complex, these five unstable domains in fungal Tom40 proteins might play an important role for the interaction with other subunits of the TOM complex in fungi.[25] It is tempting to suggest that the assembly and dissociation of the TOM complex are caused by the compensation of weakly stable regions in the TM domain of Tom40 by the association of other TOM subunits and Tom40 itself, not only in detergent buffer but also in the *in vivo* membrane environment of mitochondria.

Empirical energy calculations on AfTom40 predicted a significant stabilization of the pore protein upon mutations in β-strands 1, 7, 9, 13 and 17. However, experimental analysis revealed only a moderate resistance of the protein to chemical and thermal denaturations. A possible explanation for this is that the full-length AfTom40 construct used in this study not only comprises a β-barrel domain but also has additional large N- and C-terminal random-coil and α-helical tails. They unfold at low temperatures and low GnHCl concentrations compromising the CD and fluorescence signals of β-barrel unfolding and complicate the empirical energy calculations of the β-barrel. Another reason could be the imprecise nature of the identified locations of the 19 β-strands of AfTom40, which is used for the empirical energy calculations.

We conclude that computational prediction of unfavorable regions in β-barrel membrane proteins displays a useful tool to improve the resistance of eukaryotic β-barrel proteins to thermal and chemical denaturations. With bioinformatics-derived empirical energy parameters and calculation of thermodynamic properties based on a firm statistical mechanical model, we can now begin to combine both experimental and computational approaches to engineer β-barrel membrane proteins with rationally designed biophysical properties. We propose that our method can be easily adapted to the stabilization of other β-barrel membrane proteins, which is of high interest in, for example, nanotechnology[26] and structural biology.[27-29]

Materials and Methods

Secondary structure and weakly stable amino acid residue prediction

The software packages PRED-TMBB[30] and TMBETAPRED-RBF[31] were used for the prediction of the secondary structure of hTom40A and AfTom40. Sequence conservation and far-UV CD spectra data were incorporated in the secondary structure prediction. The oligomerization index ϱ^3 for the presumably 19-stranded β-barrel indicated the presence of higher-order protein complexes. We examined the predicted lipid-facing residues, and those with relatively higher energy values are predicted to be weakly stable. The calculation of energy values of individual β-strand residues was performed as described in Ref. 3. Briefly, we calculated the energy of each residue in the predicted native conformation using an empirical potential function, TmSIP, derived from bioinformatics analysis of β-barrel membrane proteins,[32] first developed in Refs. 20, 33 and 34 and further refined with additional structural data in Refs. 3 and 4. The energy for each residue consists of two terms. First, each residue is assigned an energy value of burying this residue type at a particular depth in the lipid bilayer and with the orientation of its side chain. There are two possible orientations, namely, side chains facing the lipid environment or facing inside the barrel. This is termed the "single-body term." Second, each residue interacts with two residues on separate neighboring strands through strong backbone H-bond interaction, side-chain interactions and weak H-bond

interactions, which collectively make up the two-body energy term. Strand energy is the summation of both single-body and two-body energy terms over all residues in the strand.

Cloning and strains

For recombinant expression of wt hTom40A in *E. coli*, a truncated version of the protein lacking amino acid residues 1–82 was used (Fig. 1a). The corresponding gene (*hTom40AΔ1–82*) was PCR amplified and cloned into a pET24d vector (Novagen) introducing a C-terminal His6-tag into the protein for purification.[35] The triple mutant *hTom40AΔ1–82*^{mut} (K107L, H117L and H220L) was prepared by site-directed mutagenesis using *hTom40AΔ1–82* as a template and Pfu Ultra II DNA Polymerase (Agilent Technologies Inc.). First, replacement of amino acids K107L and H117L was accomplished by using the primers for-K107L-H117L and rev-K107L-H117L (Supplementary Table 1). Second, to generate the mutation H220L, we further mutagenized the plasmid containing mutations K107L and H117L with primers for-H220L and rev-H220L (Supplementary Table 1). Single hTom40A mutants K107L and H117L were made by site-directed mutagenesis of *hTom40AΔ1–82* by using the primers for-H117L/rev-H117L and for-K107L/rev-K107L, respectively (Supplementary Table 1). In all cases, methylated parental plasmids were specifically digested with DpnI (New England Biolabs). Final plasmids were verified by DNA sequencing. Eventually, all vectors were transformed into *E. coli* BL21-CodonPlus (DE3) (Stratagene, Agilent Technologies) cells for protein expression.

The protein sequence of AfTom40 was retrieved from the *Aspergillus* Genome Database. The corresponding gene and an *AfTom40* gene coding for a protein with mutations K69H, N150H, S180L, S236A and K302H were synthesized and cloned into a pET24d vector (GeneArt/Invitrogen). Both genes encoded for proteins with a carboxy-terminal hexahistidine tag. To produce these AfTom40 proteins, we transformed vectors containing wt and mutant *AfTom40* into *E. coli* C41(DE3) (Lucigen) and BL21(DE3) (Stratagene, Agilent Technolgies) cells, respectively.

Protein expression and isolation of IB

wt hTom40A (hTom40AΔ1–82) and mutated hTom40A (hTom40AΔ1–82^{mut}) were expressed forming IB in *E. coli* BL21-CodonPlus (DE3) under tight control of expression from the T7 promoter. To obtain wt protein, we transformed BL21-CodonPlus (DE3) cells with pET24d-*hTom40AΔ1–82* and grew them in LB medium (20 ml) containing kanamycin (50 μg/ml) at 37 °C in shaking flasks. This culture was used to inoculate LB medium (2 l) containing kanamycin (50 μg/ml) for high-level protein expression. Protein expression was induced with 1 mM IPTG at a cell density corresponding to an OD_{600} of 0.6. After 6 h of growth, cells were harvested by centrifugation, washed with phosphate-buffered saline and stored at −20 °C until further use. Mutant hToma40A protein (hTom40AΔ1–82^{mut}) was expressed by the same procedure. For purification of wt and mutant Tom40, cells were thawed, and 3 ml lysis buffer [50 mM Tris–HCl (pH 8), 1 mM ethylenediaminetetraacetic acid, 100 mM NaCl, 1 mM phenylmethylsulfonyl fluoride (PMSF) and 0.26 mg/ml lysozyme] was added per gram of cells. After lysis of membranes with 4 mg deoxycholate per gram of cells, DNaseI (12.5 units/g cells; Sigma-Aldrich) from bovine pancreas was added.[36,37] After incubation on ice for 20 min, IB were separated from cell debris by centrifugation at 20,000*g* for 30 min at 4 °C. IB pellets were washed with buffer containing 50 mM Tris–HCl and 100 mM NaCl, pH 8, and subsequently solubilized in 6 M GnHCl, 20 mM Tris–HCl, 150 mM NaCl and 1 mM β-mercaptoethanol, pH 8, using a glass–glass homogenizer. For removal of insoluble material, the homogenate was centrifuged at 30,000*g* for 30 min at 4 °C, and supernatants were stored at 4 °C. One liter of cell culture yielded 0.5–1 g of unprocessed protein. Protein concentrations were determined by UV absorbance using an extinction coefficient ε_{280} of 29,900 M^{-1} cm^{-1} for hTom40AΔ1–82 and hTom40AΔ1–82^{mut}.[38]

For the over-expression of wt and mutant AfTom40, protein production was performed as for hTom40A with the difference that, after induction, the cells were further grown at 37 °C for 19 h and cells were harvested by centrifugation. Cell pellet was stored at −20 °C until further use (~4 g/l of cell culture). The isolation of IB was conducted under the same conditions for both AfTom40 wt and mutant and was based on the deoxycholic acid method according to Refs. 36 and 37. Cells were thawed on ice and resuspended in 30 ml of lysis buffer [50 mM Tris–HCl (pH 8.5), 1 mM ethylenediaminetetraacetic acid and 100 mM NaCl] for 10 g of cells. After the addition of PMSF and lysozyme to final concentrations of 0.13 mM and 0.26 mg/ml, respectively, solution was incubated on ice for 20 min and stirred occasionally. Then, solution was transferred into a water bath at a temperature of 37 °C. In the following, 40 mg of deoxycholic acid was added, and solution was stirred until it became viscous. Two hundred fifty units of Benzonase® (Novagen) was added at room temperature, and suspension was stirred until it was no longer highly viscous. Solution was further spun down at 19,600*g* for 30 min at 4 °C. Supernatant was discarded, and pellet was resuspended in 100 ml of TNBP buffer [50 mM Tris–HCl (pH 8.5), 100 mM NaCl, 1 mM β-mercaptoethanol and 1 mM PMSF]. After homogenization using a glass homogenizer, a clarifying spin was applied at 20,000*g* for 30 min at 4 °C. Retrieved IB pellet was resuspended in 95 ml of TNTBP buffer [TNBP buffer containing 0.1% (v/v) Triton X-100] and homogenized on ice. A second clarifying spin was applied under the same conditions. Eventually, the pellet was washed with 100 ml of TNBP buffer, and IB pellet was retrieved after centrifugation under the named conditions above. Washed IB pellet was then stored at −20 °C until further use. Determination of protein concentration was conducted as for human Tom40 by using extinction coefficients[38] ε_{280} of 37,025 M^{-1} cm^{-1} for wt and mutant AfTom40, respectively.

Protein purification and folding

IB containing wt and mutated hTom40A (hTom40AΔ1–82 and hTom40AΔ1–82^{mut}) were loaded onto a Ni-Sepharose HiTrap column (1–20 ml; GE Healthcare) equilibrated with 6 M GnHCl, 20 mM Tris–HCl, 150 mM NaCl and 1 mM β-mercaptoethanol, pH 8. After washing the column with 2 column volumes of equilibration buffer,

we removed unspecifically bound proteins with 20 mM imidazole. Then, hTom40A proteins were eluted with 300 mM imidazole, and fractions containing Tom40 were merged. Protein concentrations were adjusted to 5 mg/ml, and samples were stored at 4 °C.

For refolding of wt and mutant hTom40A, purified protein in GnHCl was diluted 10-fold into 20 mM Tris–HCl, pH 8, containing 0.5% LDAO and 1 mM β-mercaptoethanol. After removal of aggregates by centrifugation at 100,000*g*, samples containing refolded protein were concentrated to ~5 mg/ml by Ni-NTA affinity chromatography. Samples were loaded onto Ni-Sepharose HiTrap columns (1–20 ml) previously equilibrated with 20 mM Tris–HCl (pH 8), 0.1% LDAO and 1 mM β-mercaptoethanol. Bound protein was eluted in the same buffer containing 300 mM imidazole. Final purification of protein was achieved by size-exclusion chromatography using a Superose 12 column (GE Healthcare) that had been pre-equilibrated with 20 mM Tris–HCl (pH 8), 0.1% LDAO and 1 mM β-mercaptoethanol. The purity of isolated protein was assessed by SDS-PAGE followed by Coomassie Brilliant Blue staining, silver staining or Western blotting using antibodies against human Tom40 (Santa Cruz Biotechnology, Heidelberg).

For refolding of wt and mutant AfTom40A, the IB pellet of the respective protein was resuspended and homogenized in 6 ml of binding buffer [50 mM Tris–HCl (pH 7.5), 8 M urea and 1 mM β-mercaptoethanol] per gram of IB pellet. Solution was centrifuged at 19,600*g*, and supernatant was loaded onto a Ni-Sepharose HiTrap column (1–5 ml; GE Healthcare) at room temperature. After column was washed with 10–15 column volumes of binding buffer, a gradient of 0–1 M imidazole was applied. Fractions containing AfTom40 were adjusted to a protein concentration of 6 mg/ml, and 6 mg of protein was refolded in 10 ml of refolding solution [20 mM NaH_2PO_4 (pH 7), 1 mM β-mercaptoethanol and 0.8% (w/v) polyoxyethylene monolauryl ether (Brij35)]. The refolded protein solution was dialyzed at 4 °C against 50- to 100-fold volumetric excess of refolding buffer using a filter with a 6- to 8-kDa molecular mass cutoff (Spectra/Por®). Purity was then determined throughout SDS-PAGE and Coomassie Brilliant Blue. If necessary, a second purification step was conducted using the same conditions with the variation of exchanging 8 M urea against 0.8% (w/v) Brij35 in the binding and elution buffers. Purified protein was then further dialyzed against 50- to 100-fold volumetric excess of refolding buffer, and protein concentration was then adjusted to 0.2–0.4 mg/ml as needed.

Chemical cross-linking

For cross-linking experiments, 40 μg of refolded and purified hTom40AΔ1–82 and hTom40AΔ1–82^{mut} was suspended in 100 μl 20 mM NaH_2PO_4, pH 8, and incubated with 125 μM freshly prepared glutaraldehyde at 37 °C for 0–45 min. Aliquots were removed, and cross-linking reactions were stopped by adding Tris, pH 8, to a final concentration of 50 mM. Finally, cross-linking products were analyzed by SDS-PAGE and Western blotting. Polyclonal antibodies against hTom40A were obtained from Santa Cruz Biotechnology.

Circular dichroism

CD (far-UV CD) spectroscopy measurements of refolded and purified wt and mutant hTom40A (~0.2 mg/ml) in 20 mM Tris–HCl (pH 8), 1% (w/v) LDAO and 1 mM β-mercaptoethanol were performed using a Jasco J-715/815 spectrometer (Tokyo, Japan) in quartz cuvettes of 0.1-cm path length out of three independent protein preparations. Spectra were recorded at 25 °C from 185 to 260 nm with a resolution of 1.0 nm and an acquisition time of 20–100 nm/min. Final CD spectrum was obtained by averaging five consecutive scans and corrected for background by subtraction of spectrum of protein-free samples recorded under the same conditions. Melting curves were recorded at constant wavelength at 216 nm for hTom40-A(Δ1–82) wt and mutant hTom40A from 25 to a maximum of 98 °C by applying a temperature ramp of 1 °C/min. All CD samples were filtered (Rotilabo® filter; pore size, 0.22 μm) and spun down at full speed with a bench top centrifuge for 5 min at room temperature (Biofuge Fresco; Heraeus, Newport Pagnell) before measurements were conducted. Temperature readings displayed an error of ~1 °C, which was added to the experimental error. The mean residue ellipticity $\Theta(T)$ was calculated based on the molar protein concentration and the number of amino acid residues of regarding Tom40 proteins. Secondary structure content was determined using the CDpro package, namely, CDSSTR, CONTIN/LL and SELCON 3.[39-41]

AfTom40 proteins were measured under the same conditions at 0.1–0.4 mg/ml 20 mM NaH_2PO_4 (pH 7), 1 mM β-mercaptoethanol and 0.8% (w/v) Brij35.

To fit the unfolding curves of mutant Tom40, we assumed a two-state unfolding mechanism. The fraction $f_U(T)$ of unfolded protein was calculated according to $f_U(T) = [\Phi(T)-\Phi_N(T)]/[\Phi_U(T)-\Phi_N(T)]$ and fitted to the sigmoid function $f_U(T) = 1/[1+e^{(A/T-B)}]$. $\Theta_N(T)$ and $\Theta_U(T)$ represent the ellipticities of the native and unfolded molecules, respectively. At low and high temperatures, $\Theta_N(T)$ and $\Theta_U(T)$ increase linearly with temperature according to $\Theta_N(T) = aT+b$ and $\Theta_U(T) = cT+d$. A and B are fitting parameters. If unfolding is fully reversible, they correlate with enthalpic and entropic changes in the unfolding reaction, respectively.[42-44] wt Tom40 curves were fitted by superposition of two sigmoid functions assuming a three-state unfolding mechanism.[45]

Tryptophan fluorescence measurements

Tryptophan fluorescence spectra of wt and mutant hTom40A (~0.15 mg/ml) were recorded by a FP-6500 spectrofluorimeter (Jasco Inc.) after 24 h of incubation in 20 mM Tris–HCl, (pH 8), 1% (w/v) LDAO and 1 mM β-mercaptoethanol and 0.35 to 7.0 M GnHCl at 25 °C. Tryptophans were excited at 280 nm. Emission spectra were recorded between 300 and 400 nm with an integration time of 1 s. The band width for excitation and emission was set to 3 nm, respectively. Fluorescence spectra were evaluated by fitting the background-corrected spectra $I(\lambda)$ to the log-normal distribution $I(\lambda) = I_0\, e^{-[\ln 2/\ln^2 \rho]\cdot\ln^2[1+(\lambda-\lambda max)(\rho^2-1)/\rho\Gamma]}$,[46,47] where I_0 is the fluorescence intensity observed at the wavelength of maximum intensity λ_{max}, ρ is the line shape asymmetry

parameter and Γ is the spectral width at half-maximum fluorescence intensity $I_0/2$. wt and mutant AfTom40 (~0.1 mg/ml) were investigated using the same parameters in 20 mM NaH_2PO_4 (pH 7), 1 mM β-mercaptoethanol and 0.8% (w/v) Brij35.

To characterize denaturant-induced folding and unfolding of mutant hTom40A and AfTom40, we fitted the fraction of unfolded protein $f_U(D)$ by the sigmoid function f_U ([D]) = $1/[1+e^{(A-B[D])/T}]$. If unfolding and folding are fully reversible, *A* correlates with the free energy of the protein that describes its stability at zero denaturant concentration. In this case, *B* would be a measure of the dependence of free energy on denaturant concentration [D].[50-52] Chemically induced unfolding of wt Tom40 was fitted to a three-state unfolding reaction as described in the circular dichroism section.

Acknowledgements

The authors thank Drs. Uwe Gerken and Robin Ghosh for stimulating discussions and Dr. Kornelius Zeth for continuous support to F.M. We are also indebted to Drs. Andreas Kuhn and Andrei Lupas for access to the UV CD and fluorescence spectrometer and Dr. Markus Bohnsack for advice. Financial support was provided by the Competence Network on "Functional Nanostructures" of the Baden-Württemberg Foundation to S.N. and D.L. (TP/A08), by the Landesgraduiertenkolleg Baden-Württemberg to F.M., by National Institutes of Health grants GM079804 and GM086145 and National Science Foundation grant BMS0800257 to J.L., and by the Fulbright Commission and the Higher Education Commission of Pakistan to H.N.

Supplementary Data

Supplementary data associated with this article can be found, in the online version, at doi:10.1016/j.jmb.2011.07.054

References

1. Haltia, T. & Freire, E. (1995). Forces and factors that contribute to the structural stability of membrane proteins. *Biochim. Biophys. Acta*, **1228**, 1–27.
2. Stanley, A. & Fleming, K. (2007). The role of a hydrogen bonding network in the transmembrane beta-barrel OMPLA. *J. Mol. Biol.* **370**, 912–924.
3. Naveed, H., Jackups, R., Jr. & Liang, J. (2009). Predicting weakly stable regions, oligomerization state, and protein–protein interfaces in transmembrane domains of outer membrane proteins. *Proc. Natl Acad. Sci. USA*, **106**, 12735–12740.
4. Adamian, L., Naveed, H. & Liang, J. (2011). Evolutionary conservation of lipid-binding sites in membrane proteins. *Biochim. Biophys. Acta, Biomembr.* **1808**, 1092–1102.
5. Van Gelder, P., Saint, N., Phale, P., Eppens, E. F., Prilipov, A., van Boxtel, R. *et al.* (1997). Voltage sensing in the PhoE and OmpF outer membrane porins of *Escherichia coli*: role of charged residues. *J. Mol. Biol.* **269**, 468–472.
6. Phale, P. S., Philippsen, A., Kiefhaber, T., Koebnik, R., Phale, V. P., Schirmer, T. & Rosenbusch, J. P. (1998). Stability of trimeric OmpF porin: the contributions of the latching loop L2. *Biochemistry*, **37**, 15663–15670.
7. Delcour, A. (2002). Structure and function of pore-forming beta-barrels from bacteria. *J. Mol. Micro. Biotechnol.* **4**, 1–10.
8. Evanics, F., Hwang, P. M., Cheng, Y., Kay, L. E. & Prosser, R. S. (2006). Topology of an outer-membrane enzyme: measuring oxygen and water contacts in solution NMR studies of PagP. *J. Am. Chem. Soc.* **128**, 8256–8264.
9. Ahting, U., Thieffry, M., Engelhardt, H., Hegerl, R., Neupert, W. & Nussberger, S. (2001). Tom40, the pore-forming component of the protein-conducting TOM channel in the outer membrane of mitochondria. *J. Cell Biol.* **153**, 1151–1160.
10. Hill, K., Model, K., Ryan, M. T., Dietmeier, K., Martin, F., Wagner, R. & Pfanner, N. (1998). Tom40 forms the hydrophilic channel of the mitochondrial import pore for preproteins. *Nature*, **395**, 516–521.
11. Kinoshita, J. Y., Mihara, K. & Oka, T. (2007). Identification and characterization of a new tom40 isoform, a central component of mitochondrial outer membrane translocase. *J. Biochem. (Tokyo)*, **141**, 897–906.
12. Künkele, K. P., Heins, S., Dembowski, M., Nargang, F. E., Benz, R., Thieffry, M. *et al.* (1998). The preprotein translocation channel of the outer membrane of mitochondria. *Cell*, **93**, 1009–1019; issn: 0092–8674.
13. Suzuki, H., Okazawa, Y., Komiya, T., Saeki, K., Mekada, E., Kitada, S. *et al.* (2000). Characterization of rat TOM40, a central component of the preprotein translocase of the mitochondrial outer membrane. *J. Biol. Chem.* **275**, *37930–37936.*
14. Werhahn, W., Jänsch, L. & Braun, H. P. (2003). Identification of novel subunits of the TOM complex of *Arabidopsis thaliana*. *Plant Physiol. Biochem.* **41**, 407–416.
15. Bayrhuber, M., Meins, T., Habeck, M., Becker, S., Giller, K., Villinger, S. *et al.* (2008). Structure of the human voltage-dependent anion channel. *Proc. Natl Acad. Sci. USA*, **105**, 15370–15375.
16. Pusnik, M., Charriere, F., Maser, P., Waller, R. F., Dagley, M. J., Lithgow, T. & Schneider, A. (2009). The single mitochondrial porin of *Trypanosoma brucei* is the main metabolite transporter in the outer mitochondrial membrane. *Mol. Biol. Evol.* **26**, 671–680.
17. Zeth, K. (2010). Structure and evolution of mitochondrial outer membrane proteins of beta-barrel topology. *Biochim. Biophys. Acta*, **1797**, 1292–1299.
18. Becker, L., Bannwarth, M., Meisinger, C., Hill, K., Model, K., Krimmer, T. *et al.* (2005). Preprotein translocase of the outer mitochondrial membrane: reconstituted Tom40 forms a characteristic TOM pore. *J. Mol. Biol.* **353**, 1011–1020.

19. Malia, T. J. & Wagner, G. (2007). NMR structural investigation of the mitochondrial outer membrane protein VDAC and its interaction with antiapoptotic Bcl-xL. *Biochemistry*, **46**, 514–525.
20. Jackups, R., Jr. & Liang, J. (2005). Interstrand pairing patterns in beta-barrel membrane proteins: the positive-outside rule, aromatic rescue, and strand registration prediction. *J. Mol. Biol.* **354**, 979–993.
21. Suzuki, H., Kadowaki, T., Maeda, M., Sasaki, H., Nabekura, J., Sakaguchi, M. & Mihara, K. (2004). Membrane-embedded C-terminal segment of rat mitochondrial TOM40 constitutes protein-conducting pore with enriched beta-structure. *J. Biol. Chem.* **279**, 50619–50629.
22. Ahting, U., Thun, C., Hegerl, R., Typke, D., Nargang, F. E., Neupert, W. & Nussberger, S. (1999). The TOM core complex: the general protein import pore of the outer membrane of mitochondria. *J. Cell Biol.* **147**, 959–968.
23. Model, K., Meisinger, C. & Kuhlbrandt, W. (2008). Cryo-electron microscopy structure of a yeast mitochondrial preprotein translocase. *J. Mol. Biol.* **383**, 1049–1057.
24. Kato, H. & Mihara, K. (2008). Identification of Tom5 and Tom6 in the preprotein translocase complex of human mitochondrial outer membrane. *Biochem. Biophys. Res. Commun.* **369**, 958–963.
25. Sherman, E. L., Go, N. E. & Nargang, F. E. (2005). Functions of the small proteins in the TOM complex of *Neurospora crasssa*. *Mol. Biol. Cell*, **16**, 4172–4182.
26. Bayley, H. & Cremer, P. S. (2001). Stochastic sensors inspired by biology. *Nature*, **413**, 226–230.
27. Seitz, T., Bocola, M., Claren, J. & Sterner, R. (2007). Stabilisation of a (betaalpha)8-barrel protein designed from identical half barrels. *J. Mol. Biol.* **372**, 114–129.
28. Hocker, B., Lochner, A., Seitz, T., Claren, J. & Sterner, R. (2009). High-resolution crystal structure of an artificial (betaalpha)(8)-barrel protein designed from identical half-barrels. *Biochemistry*, **48**, 1145–1147.
29. Seitz, T., Thoma, R., Schoch, G. A., Stihle, M., Benz, J., D'Arcy, B. *et al.* (2010). Enhancing the stability and solubility of the glucocorticoid receptor ligand-binding domain by high-throughput library screening. *J. Mol. Biol.* **403**, 562–577.
30. Bagos, P. G., Liakopoulos, T. D., Spyropoulos, I. C. & Hamodrakas, S. J. (2004). PRED-TMBB: a web server for predicting the topology of beta-barrel outer membrane proteins. *Nucleic Acids Res.* **32**, W400–W404.
31. Ou, Y. Y., Chen, S. A. & Gromiha, M. M. (2010). Prediction of membrane spanning segments and topology in beta-barrel membrane proteins at better accuracy. *J. Comput. Chem.* **31**, 217–223.
32. Liang, J. (2002). Experimental and computational studies of determinants of membrane-protein folding. *Curr. Opin. Chem. Biol.* **6**, 878–884.
33. Jackups, R., Jr & Liang, J. (2010). Combinatorial analysis for sequence and spatial motif discovery in short sequence fragments. *IEEE/ACM Trans. Comput. Biol. Bioinform.* **7**, 524–536.
34. Jackups, R., Jr, Cheng, S. & Liang, J. (2006). Sequence motifs and antimotifs in beta-barrel membrane proteins from a genome-wide analysis: the Ala–Tyr dichotomy and chaperone binding motifs. *J. Mol. Biol.* **363**, 611–623.
35. Mager, F., Gessmann, D., Nussberger, S. & Zeth, K. (2011). Functional refolding and characterization of two Tom40 isoforms from human mitochondria. *J. Membr. Biol.* **242**, 11–21.
36. Harris, T. J., Patel, T., Marston, F. A., Little, S., Emtage, J. S., Opdenakker, G. *et al.* (1986). Cloning of cDNA coding for human tissue-type plasminogen activator and its expression in *Escherichia coli*. *Mol. Biol. Med.* **3**, 279–292.
37. Engel, J. (1987). DNA cloning: a practical approach. *Acta Biotechnol.* **9**, 254.
38. Wilkins, M., Gasteiger, E., Bairoch, A., Sanchez, J., Williams, K., Appel, R. & Hochstrasser, D. (1999). Protein identification and analysis tools in the ExPASy server. *Methods Mol. Biol. (Clifton, N. J.)*, **112**, 531–552.
39. Sreerama, N. & Woody, R. W. (2000). Estimation of protein secondary structure from circular dichroism spectra: comparison of CONTIN, SELCON, and CDSSTR methods with an expanded reference set. *Anal. Biochem.* **287**, 252–260.
40. Sreerama, N. & Woody, R. W. (2003). Structural composition of betaI- and betaII-proteins. *Protein Sci.* **12**, 384–388.
41. Sreerama, N. & Woody, R. W. (2004). Computation and analysis of protein circular dichroism spectra. *Methods Enzymol.* **383**, 318–351.
42. Becktel, W. J. & Schellman, J. A. (1987). Protein stability curves. *Biopolymers*, **26**, 1859–1877.
43. Pace, C. N., Hebert, E. J., Shaw, K. L., Schell, D., Both, V., Krajcikova, D. *et al.* (1998). Conformational stability and thermodynamics of folding of ribonucleases Sa, Sa2 and Sa3. *J. Mol. Biol.* **279**, 271–286.
44. Fersht, A. (1999). *Structure and Mechanism in Protein Science: A Guide to Enzyme Catalysis and Protein Folding*. pp. 1–631, W. H. Freeman and Company, New York.
45. Zheng, X. Y. & Yang, B. S. (2010). An improved method for measuring the stability of a three-state unfolding protein. *Chinese Sci. Bull.* **55**, 4120–4124.
46. Ladokhin, A. S., Jayasinghe, S. & White, S. H. (2000). How to measure and analyze tryptophan fluorescence in membranes properly, and why bother? *Anal. Biochem.* **285**, 235–245.
47. Winterfeld, S., Imhof, N., Roos, T., Bar, G., Kuhn, A. & Gerken, U. (2009). Substrate-induced conformational change of the *Escherichia coli* membrane insertase YidC. *Biochemistry*, **48**, 6684–6691.
48. Spyropoulos, I. C., Liakopoulos, T. D., Bagos, P. G. & Hamodrakas, S. J. (2004). TMRPres2D: high quality visual representation of transmembrane protein models. *Bioinformatics*, **20**, 3258–3260.
49. Pace, C. & Scholtz, J. (1997). Measuring the conformational stability of a protein. In *Protein Structure. A Practical Approach* (Creighton, T. E., ed.), pp. 299–321, Oxford University Press, USA.
50. Huyghues-Despointes, B. M., Pace, C. N., Englander, S. W. & Scholtz, J. M. (2001). Measuring the conformational stability of a protein by hydrogen exchange. *Methods Mol. Biol.* **168**, 69–92.
51. Myers, J. K., Pace, C. N. & Scholtz, J. M. (1995). Denaturant *m* values and heat capacity changes: relation to changes in accessible surface areas of protein unfolding. *Protein Sci.* **4**, 2138–2148.
52. Pace, C. N. (1986). Determination and analysis of urea and guanidine hydrochloride denaturation curves. *Methods Enzymol.* **131**, 266–280.